Biochemical and Biophysical Research Communications 450 (2014) 936–941

Contents lists available at ScienceDirect

Biochemical and Biophysical Research Communications

journal homepage: www.elsevier.com/locate/ybbrc

Trypanosomatid phosphoglycerate mutases have multiple conformational and oligomeric states

Elizabeth A. Blackburn [1], Fazia A.A. Fuad [1,2], Hugh P. Morgan, Matthew W. Nowicki, Martin A. Wear, Paul A.M. Michels, Linda A. Fothergill-Gilmore, Malcolm D. Walkinshaw *

Centre for Translational and Chemical Biology, School of Biological Sciences, University of Edinburgh, Edinburgh EH9 3JR, UK

ARTICLE INFO

Article history:
Received 10 June 2014
Available online 28 June 2014

Keywords:
Chemotherapeutic target
Cofactor-independent PGAM
Leishmania mexicana
SEC-MALS
Trypanosomatidae

ABSTRACT

Three structurally distinct forms of phosphoglycerate mutase from the trypanosomatid parasite *Leishmania mexicana* were isolated by standard procedures of bacterial expression and purification. Analytical size-exclusion chromatography coupled to a multi-angle scattering detector detected two monomeric forms of differing hydrodynamic radii, as well as a dimeric form. Structural comparisons of holoenzyme and apoenzyme trypanosomatid cofactor-independent phosphoglycerate mutase (iPGAM) X-ray crystal structures show a large conformational change between the open (apoenzyme) and closed (holoenzyme) forms accounting for the different monomer hydrodynamic radii. Until now iPGAM from trypanosomatids was considered to be only monomeric, but results presented here show the appearance of a dimeric form. Taken together, these observations are important for the choice of screening strategies to identify inhibitors of iPGAM for parasite chemotherapy and highlight the need to select the most biologically or functionally relevant form of the purified enzyme.

1. Introduction

The search for chemotherapeutic targets in parasites of the Trypanosomatidae family (comprising the *Trypanosoma* and *Leishmania* genera) has identified the glycolytic enzyme, phosphoglycerate mutase (PGAM) as an attractive prospect [1]. This enzyme occurs in two taxon-specific versions which share no structural or mechanistic similarities. Both versions catalyse the interconversion between 2-phosphoglycerate (2PGA) and 3-phosphoglycerate (3PGA). PGAM in humans belongs to the cofactor-dependent version (dPGAM), whereas the enzyme from trypanosomatids is the alternative cofactor-independent version (iPGAM) [2,3]. Moreover, it is known that the pathogenic bloodstream stage of *Trypanosoma brucei* is completely dependent on the catabolism of glucose to pyruvate via the glycolytic pathway for the production of ATP [4–6]. In addition, RNAi experiments have shown that an approximately 50% reduction in the intracellular level of PGAM in *T. brucei* (*Tb*PGAM) is sufficient to cause death of cultured parasites [7].

Human dPGAM is a dimeric enzyme that occurs in two tissue-specific isoenzymes. Both isoenzymes are dependent on 2,3-bisphosphoglycerate for activity, and involve a phosphohistidine intermediate at the active site. Similar dPGAMs are found in vertebrates, amphibians, yeasts and certain bacteria. By contrast, iPGAMs occur in plants, many protists including kinetoplastids which comprise the Trypanosomatidae, nematodes, algae and certain other bacteria. These are monomeric two-domain enzymes which require divalent metals for activity, and involve a phosphoserine intermediate [8–11].

Analysis of the amino-acid sequences of iPGAMs shows that they may be grouped into two families (Fig. S1 and Table S1). iPGAMs from plants and trypanosomatids comprise family 1, with the remaining enzymes in family 2. X-ray crystal structures are available for *Leishmania mexicana* PGAM [11] and for *Tb*PGAM from family 1 [12], and for *Geobacillus stearothermophilus* [13], *Staphylococcus aureus* (4MY4.pdb) and *Bacillus anthracis* from family 2 [14]. The crystallographic data show that both family 1 and family 2 iPGAMs can be trapped in open and closed monomeric forms. In the present study we investigated which conformational and oligomeric states of *Lmi*PGAMs are present in solution. These findings are of particular relevance for the choice of screening strategies to identify inhibitors of iPGAMs with a view to drug discovery and development.

* Corresponding author.
E-mail address: m.walkinshaw@ed.ac.uk (M.D. Walkinshaw).
[1] These authors contributed equally to the work.
[2] Present address: Institute for Research in Molecular Medicine, Universiti Sains Malaysia, 16150 Kubang Kerian, Kelantan, Malaysia.

http://dx.doi.org/10.1016/j.bbrc.2014.06.113
0006-291X/

2. Materials and methods

2.1. Materials

3PGA, enolase (baker's yeast) and pyruvate kinase (rabbit muscle) were obtained from Sigma–Aldrich; lactate dehydrogenase (LDH, rabbit muscle) from Fluka Analytical. *Escherichia coli* competent cells were from Novagen. Prepacked chromatography columns were obtained from GE Healthcare, and Vivaspin columns from Sartorius Stedim Biotech.

2.2. Expression and purification of LmPGAM

Chemically competent *E. coli* BL21(DE3) cells were transformed with pET28a*Lm*PGAM (C-terminal His-tag; LEHHHHHH)[10]. Cells were grown in 2xTY medium containing kanamycin (50 μg mL^{-1}); 250 rpm shaking and expression induced for 18 h, 291 K, 1 mM IPTG. Cell pellets were re-suspended in 50 mM NaH_2PO_4, pH 8.0, 300 mM NaCl, 20 mM imidazole, 10% glycerol and EDTA-free protease inhibitor (1 tablet/1 L cell culture equivalent; Roche) and lysed with a Constant Systems 1.1 kW TS Cell Disruptor (set to 25 kPsi; 172 MPa). After centrifugation the supernatant was loaded onto a 5 mL IMAC Hitrap HP column, pre-charged with nickel and washed with ten column volumes (CV) of buffer A (50 mM NaH_2PO_4, pH 8.0, 300 mM NaCl and 20 mM imidazole) followed by 15 CV 10% buffer B (50 mM NaH_2PO_4, pH 8.0, 300 mM NaCl, and 500 mM imidazole). The *Lm*PGAM protein was eluted with a 10 CV step gradient (10–100% buffer B). Fractions containing *Lm*PGAM were buffer exchanged into 20 mM HEPES, pH 7.6 and 1 mM DTT (Hiprep 26/10 desalting) and loaded onto a Mono Q 5/50 GL ion-exchange column. The protein was eluted over a 15 CV gradient with buffer D (20 mM HEPES, pH 7.6, 1 M NaCl and 1 mM DTT). *Lm*PGAM eluted as three distinct peaks; Iex1 (217 mM NaCl), Iex2 (253 mM NaCl), Iex3 (303 mM NaCl). Samples containing *Lm*PGAM were pooled into three fractions (Iex1, Iex2, Iex3), concentrated (1 mg mL^{-1}) and separately loaded onto a Superdex 200 10/300 GL column pre-equilibrated with 20 mM triethanolamine (TEA–HCl), pH 7.6, 50 mM NaCl. Final purity was greater than 95%.

2.3. Enzyme assay

Continuous coupled iPGAM assays were performed using a Multimode Plate Reader-Molecular Devices M5 instrument, by the addition of 10 μL of iPGAM sample (0.02 mg mL^{-1}) to give a final reaction mixture of 100 μL containing 100 mM TEA–HCl buffer pH 7.6, 1.5 mM 3PGA, 5 mM $MgCl_2$, 50 mM KCl, 0.8 mM NADH, 1 mM ADP, 2 units of enolase, 4 units of pyruvate kinase and 6 units of LDH. The decreased absorbance of NADH over time at A_{340} nm was used to obtain the rate of reaction for specific activity measurements (one unit corresponds to the conversion of 1 μmol of substrate min^{-1} mg^{-1} protein at 298 K) [15].

2.4. SEC-MALS analysis

Size-Exclusion Chromatography coupled to a DAWN HELIOS II™ MALS instrument (Wyatt Technology) and Optilab T-rEX refractometer (Wyatt Technology) was used to determine the molar mass of the proteins in the three ion-exchange fractions. 100 μL of 1 mg mL^{-1} (16 μM) of each *Lm*PGAM ion-exchange fraction was loaded onto on a Superdex 200 10/300 GL column pre-equilibrated with 20 mM TEA–HCl, pH 7.6, 50 mM NaCl, at a flow rate of 0.5 mL min^{-1}, 293 K; elution monitored by absorbance at 280 nm. The on-line measurement of the intensity of the Rayleigh scattering was used to determine the weight average molecular masses (M_w) of the eluted proteins, using the ASTRA™ software (Wyatt Technology). Experiments were repeated in triplicate.

2.5. Structural analyses

Superpositions of iPGAM structures were performed using PyMOL (http://www.pymol.org/) and CCP4 SUPERPOSE [16,17]. The rigid body rotations were calculated by simultaneously superposing the phosphatase domain (residues 3–88 and 332–551) of the *Tb*PGAM apoenzyme (PDB ID 3NVL) and *Lm*PGAM holoenzyme (PDB ID 3IGY) structures (RMS fit of the C-α atoms is 0.5 Å). The resulting coordinates were recorded for both structures. Using the new coordinates, CCP4 SUPERPOSE was used to superpose the transferase domain of the apoenzyme onto the holoenzyme structure (the average RMS fit of the C-α atoms for each chain is 0.3 Å), providing both the centroid and the rotation matrix.

The predicted hydrodynamic properties of the protein molecules were obtained from the program HYDROPRO10 [18]. DYNDOM [19] was used to investigate the molecular movements between the open and closed forms of iPGAM, and the program Surface Triplet Propensities (STP) [20] was used to predict the most likely areas on the iPGAM monomer surface that may interact with another monomer to form a dimer (http://opus.bch.ed.ac.uk/stp/). PISA [21] was also used to study the potential interface between monomers to form dimeric iPGAM.

3. Results and discussion

3.1. Ion-exchange chromatography separates LmPGAM into active forms with different hydrodynamic properties

Bacterially expressed His-tagged *Lm*PGAM has previously been conveniently purified in high yields using a cobalt IMAC column [3,10,22]. The presence of cobalt has been shown to hyper-activate iPGAM, though it is unlikely to be biologically relevant [15]. This has prompted us to redesign the purification protocol. The new protocol for C-terminal $(His)_6$*Lm*PGAM (pI 5.4) uses a nickel (IMAC) column followed by separation on a MonoQ 5/50 GL column into three distinct peaks Iex1, Iex2 and Iex3 (Fig. 1A).

The specific activities of Iex1, Iex2 and Iex3 were 20.0, 19.8 and 15.9 μmol min^{-1} mg^{-1}, respectively. These activities are similar to that of *Tb*PGAM purified through a nickel IMAC column (26 μmol min^{-1} mg^{-1}, [9]). As the activities of the three different forms were quite similar, we were interested in how structural differences could explain the different forms of PGAM. Fractions of each of the three ion-exchange peaks (Iex1, Iex2, Iex3) were pooled separately, concentrated to 1 mg/mL and further analysed by analytical gel filtration. Iex1 and Iex2 eluted as single peaks with retention volumes of 13.89 ± 0.03 and 13.38 ± 0.02 mL, respectively. Under identical conditions Iex3 eluted as two distinct species with retention volumes of 11.62 ± 0.02 (minor peak) and 13.37 ± 0.02 (major peak) mL (Fig. 1B).

Size-exclusion chromatography separates proteins on the basis of their hydrodynamic volume. For similarly shaped particles there are linear relationships between the hydrodynamic radius, R_h, and $\sqrt{\log(K_{av})}$ (where K_{av} is the partition coefficient) and between R_h and $logM_r$. Elution positions of *Lm*PGAM from SEC were compared to calibration curves of well characterised globular protein standards to determine whether Iex1, Iex2 or Iex3 had hydrodynamic properties that equated to a globular monomeric form (Fig. 1B). The calculated R_h values were: Iex1, 32.9 Å (64.1 kDa); Iex2, 35.7 Å (81.0 kDa); Iex3, 46.9 Å (184.1 kDa) and 35.8 Å (81.56 kDa) (Fig. S2).

SDS–PAGE could not distinguish between any of these forms of *Lm*PGAM (Fig. S3) as all ran at the same position close to the calculated mass of 61.8 kDa. Therefore only Iex1 approximates to the

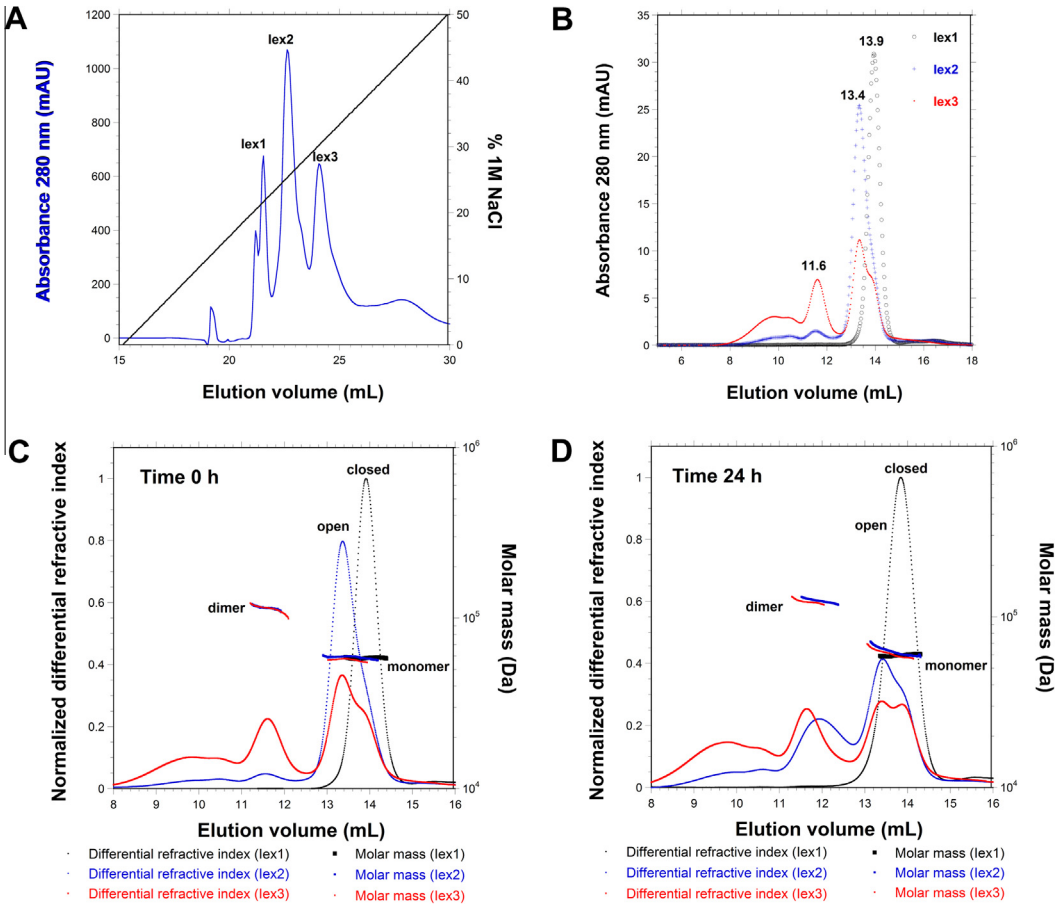

Fig. 1. *Lm*PGAM exists in more than one conformation. (A) Gradient elution of three distinct *Lm*PGAM peaks (Iex1, Iex2 and Iex3) from a MonoQ 5/50GL column. (B) Gel-filtration UV absorbance elution profile at 280 nm observed for *Lm*PGAM samples Iex1 (black), Iex2 (blue) and Iex3 (red). (C) SEC-MALS elution profile showing differential refractive index and absolute molecular mass determination for Iex1 (black), Iex2 (blue) and Iex3 (red) at time 0 h, and (D) at time 24 h. (For interpretation of the references to colour in this figure legend, the reader is referred to the web version of this article.)

globular monomeric form of the enzyme. Iex2 and Iex3 contain PGAM with larger hydrodynamic volumes than Iex1. This indicates that there is more than one active form of the enzyme that may be trapped under certain conditions, and that the larger species do not represent misfolded inactive forms as each form had comparable specific activity.

3.2. Characterisation of multiple forms of iPGAM by SEC-MALS

iPGAMs are known to crystallise as open and closed monomeric forms that may reflect functionally significant low energy conformations [11,14,22]. Molecular dynamic simulations starting with the crystal structure of the family 2 iPGAM from *B. anthracis* (*Ba*PGAM) predict a significant kinetic barrier to conversion between open and closed forms [14]. Hydrodynamic radii calculated from these X-ray structures are compared with values derived from gel filtration experiments (Table 1).

We hypothesised that our ion-exchange and size-exclusion chromatography purification strategy separated a dimeric and two monomeric forms of the protein. To test this, absolute molecular mass determination was performed by SEC-MALS on the three ion-exchange fractions (Iex1, Iex2 and Iex3) (Fig. 1B). The experiment was repeated after 16 and 24 h to determine if there was significant inter-conversion between the different species.

Fig. 1C and D illustrate the elution profiles for Iex1, Iex2 and Iex3, and the absolute molecular mass estimates. Iex1 represents the species with the smallest hydrodynamic radius as indicated by the retention time on the SEC column. SEC-MALS showed that Iex1 contained a species with a mass of 58.6 ± 0.8 kDa, close to the calculated mass of His-tagged monomeric *Lm*PGAM (61.8 kDa). The SEC-MALS elution profiles for the smallest iPGAM form in Iex1 do not show a significant change over the time course of the experiment and have a consistent elution volume of 13.89 ± 0.02 mL. The major component of Iex2 represents a species with a slightly larger hydrodynamic radius than that of Iex1. SEC-MALS confirmed the major species in the Iex2 fraction to be monomeric, with a mass of 60.67 ± 2.1 kDa (Fig. 1C and D). The change in hydrodynamic radii of the monomeric peaks from Iex1 and Iex2 can be accounted for by a difference in protein conformation.

We propose that the major species present in Iex1 and Iex2 represent closed and open forms of monomeric *Lm*PGAM, respectively. In addition, Iex2 at time 0 contains a trace of dimeric *Lm*PGAM with a mass of 121.13 ± 5.4 kDa (calculated dimer mass 123.58 kDa). The major species is the open form of the monomer, with a shoulder representing the closed form. The SEC-MALS data showed that Iex3 contains a mixture of both monomeric and dimeric forms with masses of 59.21 ± 2.09 and 118.77 ± 4.77 kDa respectively (Fig. 1C and D). The monomer to dimer ratio in Iex3 is approximately 2:1. Interestingly, there appears to be a slow interconversion between the open monomeric and dimeric forms of *Lm*PGAM (Fig. 1C and D). The Iex2 sample has a time-dependent shift towards a larger proportion of the dimeric form. After 24 h the ratio of open monomer to dimer has shifted from 20:1 to 2:1. The same pattern is reproduced in the Iex3 sample; the dimeric form increases relative to the open monomeric form, and the closed monomeric form appears to remain constant.

Table 1
Hydrodynamic properties of *Tb*PGAM, SaPGAM, *Lm*PGAM, *Ba*PGAM and *Gs*PGAM calculated from X-ray crystallographic coordinates using the program HYDROPRO10: temperature 293 K; solvent viscosity 9.84×10^{-4} Pa s, atomic radius 2.9 Å. Ticks indicate the presence of 2PGA or 2PGA. Mass of PGAM in crystallographic representation is quoted.

Organism	PDB ID	Family	Form	3PGA	2PGA	M1	M2	Shape factor, ρ (R_g/R_h)	Hyd. radius, R_h (Å)	Radius gyration, R_g (Å)	Volume (Å^3)	Mass (kDa)
*Tb*PGAM	3NVL	1	Open	×	×	Co	Co	0.799	32.93	26.30	9.919×10^4	60.4
*Sa*PGAM	4MY4	2	Open	×	×	Mn	Mn	0.822	32.13	26.40	9.170×10^4	56.2
*Ba*PGAM	2IFY	2	Open	×	×	Mn	Mn	0.843	32.84	27.68	9.169×10^4	56.1
*Lm*PGAM	3IGY	1	Closed	✓	✓	Co	Co	0.776	32.06	24.87	9.833×10^4	60.3
*Gs*PGAM	1EJJ	2	Closed	✓	×	Mn	Mn	0.779	30.87	24.04	9.074×10^4	56.6
*Gs*PGAM	1EQJ	2	Closed	×	✓	Mn	Mn	0.780	30.85	24.05	9.055×10^4	56.6
*Gs*PGAM	1O98	2	Closed	×	✓	Mn	Mn	0.777	31.45	24.45	9.546×10^4	56.8
*Gs*PGAM	1O99	2	Closed	×	✓	Mn		0.775	31.48	24.40	9.536×10^4	56.8

3.3. Ion-exchange chromatography separates closed from open and dimeric forms of LmPGAM

The crystal structures of iPGAM were analysed using the program HYDROPRO10 [18] (Table 1). HYDROPRO10 predicts hydrodynamic properties and the radius of gyration, R_g, from 3D coordinates. The shape factor ratio R_g/R_h is a useful metric to compare 3D protein structures. Globular proteins have R_g/R_h close to 0.775 [23]; as the shape becomes more elongated R_g increases relative to R_h and R_g/R_h increases. From the crystallographic data of the closed forms of both family 1 and family 2 iPGAMs, the R_g/R_h is remarkably similar and very close to 0.78 as expected from their essentially globular structures. The more elongated open crystallographic forms of family 2 iPGAMs have larger R_g/R_h values of 0.822 and 0.843 as would be predicted from visualisation of the structures. The value for the open form of the family 1 *T. brucei* iPGAM is lower (0.799), consistent with its more compact shape when compared to the family 2 enzymes. When hydrodynamic radii are compared for the crystallographic data and for the open and closed forms of the monomeric forms of *Lm*PGAM calculated from the SEC elution positions, the closed monomeric form, Iex1, has a radius of 32.9 Å (Fig. S2), close to that which would be predicted from the mass for a globular protein. The open monomeric form, Iex2, has a very much larger hydrodynamic radius (35.7 Å) from the SEC elution position.

The crystallographic data show that structures with either 3PGA or 2PGA in the active site are in the closed form. The apoenzyme structures are all open, and differ in degree of openness between family 1 and 2 enzymes (Table 1).

3.4. Regulation of open and closed forms of iPGAM by substrate

The analysis presented in Fig. S1 and Table S1 shows that iPGAMs from *T. brucei* and *L. mexicana* share 78% amino-acid sequence identity, and possess a constellation of sequence features characteristic of family 1 iPGAMs. A comparison of the crystal structures of *Lm*PGAM in its closed holoenzyme conformation [11] with that of *Tb*PGAM in its open apoenzyme conformation [12] is presented in Fig. 2. Both enzymes possess a typical two-domain structure, comprising a phosphatase domain and a transferase domain (Fig. 2A). In the holoenzyme structure, the two domains are clamped together to enclose the substrate binding site and two metal binding sites, with active site residues contributed by both domains.

The phosphatase domain of the apoenzyme form of *Tb*PGAM superposes onto the phosphatase domain of the holoenzyme form of *Lm*PGAM (Fig. 2A and B) with a RMS fit for the Cα atoms of 0.5 Å. Superposition of the transferase domains gives a RMS fit of 0.3 Å. The program DynDom [19] was used to calculate the angle of rotation of the transferase domain in relation to the phosphatase domain, which takes place at residues 89–90 (QG) and 329–336 (LVPPPKLTR), which are conserved in both enzymes (Fig. S1). The proline residues in the latter sequence are classic indicators of a hinge region. With the phosphatase domain fixed in both structures, the transferase domain rotates by 67° upon substrate binding (Fig. 2B). In the apoenzyme structure the active site is exposed, but substrate binding provokes the rigid body rotation of the transferase domain (when the phosphatase domain is fixed) thereby occluding the active site (Fig. 2B).

The open/apoenzyme form of bacterial family 2 iPGAM is quite distinct from the open/apoenzyme form of trypanosomatid family 1 iPGAM, and the transition between the closed and open forms is consequently very different. In the previously published open structure of *Ba*PGAM [only 35% identical to *Tb*PGAM and 33% identical to *Lm*PGAM (Fig. S1 and Table S1)], the cleft separating the two domains is extremely wide [14] in comparison to the trypanosomatid structures, suggesting greater flexibility in the linker region. Indeed this would appear to be the case as the hinge region of the trypanosomatid iPGAMs encompasses three conserved consecutive proline residues (331, 332 and 333). These residues are consistent with the apparently different opening–closing mechanism of trypanosomatid iPGAMs, whereby the transferase domain rotates (like screwing the lid of a jar) towards the phosphatase domain, making the transition from apoenzyme to holoenzyme. By comparison the domains of the bacterial family 2 iPGAMs experience a relatively simple hinging motion with minimal rotation, rather like the movement of the wings of a butterfly.

3.5. STP and PISA analyses identify a possible dimeric PGAM interface

The appearance of a dimeric species in solution as shown by the SEC-MALS results led us to examine the structures of trypanosomatid PGAMs for possible dimer formation using the programs STP [20] and PISA [17,21]. The STP analysis of the holoenzyme form of *Lm*PGAM identified surfaces with an above average propensity to form inter-molecular interactions (Fig. S4B and C), in particular, regions contiguous to the side chain of Asp32 and around the entry surface into the active site. The region around Asp32, characterised by a cluster of acidic amino acids, is seen in both *Tb* and *Trypanosoma cruzi* iPGAM and was also identified by PISA (Fig. S1).

3.6. Druggability of iPGAM

iPGAM from trypanosomatids has been identified as an attractive chemotherapeutic target because the glycolytic pathway is essential for ATP production. Moreover, the enzyme is completely different from its human counterpart, and is present at relatively low activity within parasite cells. However, the active site of the closed form of the enzyme is small, hydrophilic and inaccessible and may therefore be only poorly druggable. Fortunately it is known from the results presented in this paper and by previous work on trypanosomatid iPGAMs that these enzymes may exist in an open conformation whereby the region between the two domains forms an accessible larger and chemically more diverse

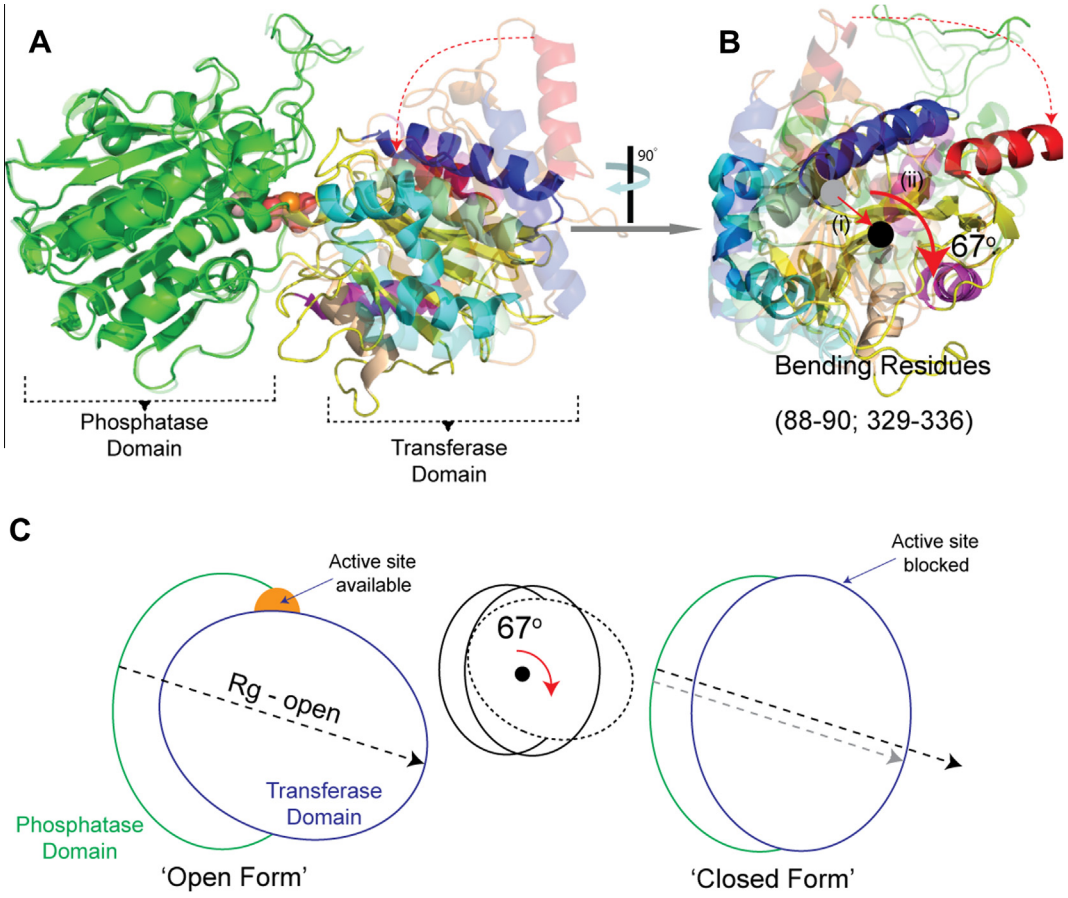

Fig. 2. Open and closed forms of monomeric *Lm*PGAM. (A–B) Two views of the superposed apo-*Tb*PGAM and holo-*Lm*PGAM monomers. The phosphatase domains of both enzymes were superposed to highlight the different conformations of the transferase domains observed between the apoenzyme (open – increased transparency) and holoenzyme (closed) structures. Helices are coloured as follows (numbered according to the *Lm*PGAM structure); residues 92–118 and 139–151 (pale green); residues 171–191 (blue); residues 213–225 and 234–246 (red); residues 285–294 (wheat). The substrate and metal ion (represented as spheres) are shown bound to the active site, which forms when both the transferase and phosphatase domains meet. (B) The apoenzyme (open) to holoenzyme (closed) transition: the direction of the calculated 67° rigid body rotation (ii) of the transferase domain (shown by a curved red arrow) with a concomitant translation of the centre of gyration ((i) grey and black dots). (C) A schematic representation of the open to closed transition, showing changes to the radius of gyration (*Rg*), grey and black dashed arrows indicate relative sizes. In the open form the active site is exposed allowing for substrate binding and product release. A rigid body rotation of the transferase domain closes the active site, allowing for the inter-conversion of 3- and 2-phosphoglycerates. (For interpretation of the references to colour in this figure legend, the reader is referred to the web version of this article.)

cavity which may indeed be druggable. It would seem likely that substrate and cofactors binding to iPGAM are ligands that may perturb the equilibrium between open, closed and dimeric forms. It is perhaps not surprising that high-throughput screening protocols which use a standard continuous enzyme assay coupled to enolase, pyruvate kinase and LDH suggest that family 2 iPGAMs from nematodes have limited druggability [24]. The design of screening strategies should therefore address the need to provide conditions which favour the open conformation of the enzyme.

Acknowledgments

Fazia A.A. Fuad was funded by the Ministry of Higher Education, Malaysia and the University of Science Malaysia. The Centre for Translational and Chemical Biology and the Edinburgh Protein Production Facility were funded by the Wellcome Trust and the Biotechnology and Biological Sciences Research Council.

Appendix A. Supplementary data

Supplementary data associated with this article can be found, in the online version, at http://dx.doi.org/10.1016/j.bbrc.2014.06.113.

References

[1] C.L.M.J. Verlinde, V. Hannaert, C. Blonski, et al., Glycolysis as a target for the design of new anti-trypanosome drugs, Drug Resist. Updat. 4 (2001) 50–65.
[2] L.A. Fothergill-Gilmore, P.A.M. Michels, Evolution of glycolysis, Prog. Biophys. Mol. Biol. 59 (1993) 105–235.
[3] N. Chevalier, D.J. Rigden, J. Van Roy, et al., *T. brucei* contains a 2,3-bisphosphoglycerate independent phosphoglycerate mutase, Eur. J. Biochem. 267 (2000) 1464–1472.
[4] J.F. Ryley, Studies on the metabolism of the Protozoa, Biochem. J. 62 (1956) 215–222.
[5] P.T. Grant, J.D. Fulton, The catabolism of glucose by strains of *Trypanosoma rhodesiense*, Biochem. J. 66 (1957) 242–250.
[6] J.R. Haanstra, A. van Tuijl, J. van Dam, et al., Proliferating bloodstream-form *T. brucei* use a negligible part of consumed glucose for anabolic processes, Int. J. Parasitol. 42 (2012) 667–673.
[7] M.-A. Albert, J.R. Haanstra, V. Hannaert, et al., Experimental and *in silico* analyses of glycolytic flux control in bloodstream form *Trypanosoma brucei*, J. Biol. Chem. 280 (2005) 28306–28315.
[8] M. Jedrzejas, M. Chander, P. Setlow, et al., Mechanism of catalysis of cofactor-independent phosphoglycerate mutase from *B. stearothermophilus*, J. Biol. Chem. 275 (2000) 23146–23153.
[9] J.-F. Collet, V. Stoobant, E. Van Schaftingen, The 2,3-bisphosphoglycerate-independent phosphoglycerate mutase from *Trypanosoma brucei*, FEMS Microbiol. Lett. 204 (2001) 39–44.
[10] D.G. Guerra, D. Vertommen, L.A. Fothergill-Gilmore, et al., Characterization of the cofactor-independent phosphoglycerate mutase from *L. mexicana*, Eur. J. Biochem. 271 (2004) 1798–1810.
[11] M.W. Nowicki, B. Kuaprasert, I.W. McNae, et al., Crystal structures of *L. mexicana* phosphoglycerate mutase suggest a one-metal mechanism and a new enzyme subclass, J. Mol. Biol. 394 (2009) 535–543.

[12] G.F. Mercaldi, H.M. Pereira, A.T. Cordeiro, et al., Structural role of the active-site metal in the conformation of *T. brucei* phosphoglycerate mutase, FEBS J. 279 (2012) 2012–2021.
[13] M. Jedrzejas, M. Chander, P. Setlow, et al., Structure and mechanism of action of a novel phosphoglycerate mutase from *B. stearothermophilus*, EMBO J. 19 (2000) 1419–1431.
[14] M. Nukui, L.V. Mello, J.E. Littlejohn, et al., Structure and molecular mechanism of *B. anthracis* cofactor-independent phosphoglycerate mutase, Biophys. J. 92 (2007) 977–988.
[15] F.A.A. Fuad, L.A. Fothergill-Gilmore, M.W. Nowicki, et al., Phosphoglycerate mutase from *T. brucei* is hyperactivated by cobalt *in vitro*, but not *in vivo*, Metallomics 3 (2011) 1310–1317.
[16] E. Potterton, P. Briggs, M. Turkenburg, et al., A graphical user interface to the CCP4 program suite, Acta Crystallogr. D Biol. Crystallogr. 59 (2003) 1131–1137.
[17] E. Krissinel, K. Henrick, Secondary-structure matching (SSM), a new tool for fast protein structure alignment in three dimensions, Acta Crystallogr. D Biol. Crystallogr. 60 (2004) 2256–2268.
[18] A. Ortega, D. Amoros, J. Garcia de la Torre, Prediction of hydrodynamic and other solution properties of rigid proteins from atomic- and residue-level models, Biophys. J. 101 (2011) 892–898.
[19] S. Hayward, H.J.C. Berendsen, Systematic analysis of domain motions in proteins from conformational change, Proteins 30 (1998) 144–154.
[20] W. Mehio, G.J.L. Kemp, P. Taylor, et al., Identification of protein binding surfaces using surface triplet propensities, Bioinformatics 26 (2010) 2549–2555.
[21] E. Krissinel, K. Henrick, Inference of macromolecular assemblies from crystalline state, J. Mol. Biol. 372 (2007) 774–797.
[22] B. Poonperm, D.G. Guerra, I.W. McNae, et al., Expression, purification, crystallization and preliminary crystallographic analysis of *L. mexicana* phosphoglycerate mutase, Acta Crystallogr. D Biol. Crystallogr. 59 (2003) 1313–1316.
[23] W. Burchard, M. Schmidt, W.H. Stockmayer, Information on polydispersity and branching from combined quasi-elastic and integrated scattering, Macromolecules 13 (1980) 1265–1272.
[24] G.J. Crowther, M.L. Booker, M. He, et al., Cofactor-independent phosphoglycerate mutase from nematodes has limited druggability, as revealed by two high-throughput screens, PLOS Negl. Trop. Dis. 8 (2014) e2628.